Cell Death and Differentiation (2016) 23, 1515–1528
 1350-9047/16
www.nature.com/cdd

p53 isoforms regulate astrocyte-mediated neuroprotection and neurodegeneration

C Turnquist[1], I Horikawa[1], E Foran[2], EO Major[3], B Vojtesek[4], DP Lane[5], X Lu[6], BT Harris*[,7,8,9] and CC Harris*[,1,9]

Bidirectional interactions between astrocytes and neurons have physiological roles in the central nervous system and an altered state or dysfunction of such interactions may be associated with neurodegenerative diseases, such as Alzheimer's disease (AD) and amyotrophic lateral sclerosis (ALS). Astrocytes exert structural, metabolic and functional effects on neurons, which can be either neurotoxic or neuroprotective. Their neurotoxic effect is mediated via the senescence-associated secretory phenotype (SASP) involving pro-inflammatory cytokines (e.g., IL-6), while their neuroprotective effect is attributed to neurotrophic growth factors (e.g., NGF). We here demonstrate that the p53 isoforms Δ133p53 and p53β are expressed in astrocytes and regulate their toxic and protective effects on neurons. Primary human astrocytes undergoing cellular senescence upon serial passaging *in vitro* showed diminished expression of Δ133p53 and increased p53β, which were attributed to the autophagic degradation and the SRSF3-mediated alternative RNA splicing, respectively. Early-passage astrocytes with Δ133p53 knockdown or p53β overexpression were induced to show SASP and to exert neurotoxicity in co-culture with neurons. Restored expression of Δ133p53 in near-senescent, otherwise neurotoxic astrocytes conferred them with neuroprotective activity through repression of SASP and induction of neurotrophic growth factors. Brain tissues from AD and ALS patients possessed increased numbers of senescent astrocytes and, like senescent astrocytes *in vitro*, showed decreased Δ133p53 and increased p53β expression, supporting that our *in vitro* findings recapitulate *in vivo* pathology of these neurodegenerative diseases. Our finding that Δ133p53 enhances the neuroprotective function of aged and senescent astrocytes suggests that the p53 isoforms and their regulatory mechanisms are potential targets for therapeutic intervention in neurodegenerative diseases.
Cell Death and Differentiation (2016) **23,** 1515–1528; doi:10.1038/cdd.2016.37; published online 22 April 2016

Brain aging and neurodegenerative diseases remain major medical challenges of the twenty-first century. Alzheimer's disease (AD), the most common form of dementia, affects about 36 million people worldwide and is estimated to have cost $604 billion in 2010 alone.[1] Amyotrophic lateral sclerosis (ALS) is characterized by the loss of upper and lower motor neurons and life expectancy is 2–5 years following diagnosis. It is estimated to affect about 500 000 individuals in the USA alone and costs are $256–$433 million per year.[2] Despite continued scientific effort, few effective therapies exist for these neurodegenerative diseases.

Astrocytes are the most abundant cell type in the brain and have key roles in providing structural, functional, and metabolic support to neurons.[3] Although AD and ALS possess different etiologies, a commonality between these two diseases is the role of astrocytes in neurodegeneration.[4,5] Dysfunctional neuron–astrocyte crosstalk is known to be a central feature of neurodegenerative diseases.[6,7] Astrocytes exert both toxic and protective effects on neurons in a context-dependent manner. The neurotoxic effects of astrocytes are mediated in part through pro-inflammatory cytokines, such as interleukin-6 (IL-6). Overproduction of these factors is associated with human neurodegeneration[8] and murine models.[9] The neuroprotective effects of astrocytes are mediated through nerve growth factor (NGF) and insulin-like growth factor-1 (IGF-1),[10] which are deficient in neurodegenerative diseases[11,12] and, to a lesser extent, during physiological brain aging.[13] Alexander disease, a rare astrocyte disease

[1]Laboratory of Human Carcinogenesis, Center for Cancer Research, National Cancer Institute, National Institutes of Health, Bethesda, MD 20892, USA; [2]Neurogenetics Branch, National Institute of Neurological Disorders and Stroke, National Institutes of Health, Bethesda, MD 20892, USA; [3]Laboratory of Molecular Medicine and Neuroscience, National Institute of Neurological Disorders and Stroke, National Institutes of Health, Bethesda, MD, USA; [4]Regional Centre for Applied and Molecular Oncology, Masaryk Memorial Cancer Institute, Brno 65653, Czech Republic; [5]p53 Laboratory, Biomedical Sciences Institutes (A*STAR), Singapore 138648, Singapore; [6]Ludwig Institute for Cancer Research, Nuffield Department of Clinical Medicine, University of Oxford, Oxford OX3 7DQ, UK; [7]Department of Neurology, Georgetown University Medical Center, Washington DC 20007, USA and [8]Department of Pathology, Georgetown University Medical Center, Washington DC 20007, USA
*Corresponding author: BT Harris, Departments of Neurology and Pathology, Georgetown University Medical Center, 4000 Reservoir Road, NW, Building D, Room 207, Washington, DC 20057, USA. Tel: 202 687 5345; Fax: 202 687 7378; E-mail: Bth@georgetown.edu
or CC Harris, Laboratory of Human Carcinogenesis, Center for Cancer Research, National Cancer Institute, National Institutes of Health, 37 Convent Drive, Room 3068A, Bethesda, MD 20892, USA. Tel: 301 496 2048; Fax: 301 496 0497; E-mail: Curtis_Harris@nih.gov
[9]These authors contributed equally to this work.

Abbreviations: AD, Alzheimer's disease; ALS, amyotrophic lateral sclerosis; DAPI, 4′,6-diamidino-2-phenylindole; EAAT2, excitatory amino acid transporter-2; GFAP, glial fibrillary acidic protein; IGF-1, insulin-like growth factor-1; IL, interleukin; IL-6-NAb, IL-6 neutralizing antibody; iPSC, induced pluripotent stem cell; NGF, nerve growth factor; NGF-NAb, NGF neutralizing antibody; NOS2, nitric oxide synthase 2; SA-β-Gal, senescence-associated β-galactosidase; SASP, senescence-associated secretory phenotype; γH2AX, phosphorylated H2AX

Received 23.10.15; revised 11.3.16; accepted 19.3.16; Edited by N Bazan; published online 22.4.2016

involving a mutation in the glial fibrillary acidic protein (GFAP), results in neurodegeneration.[14] Riluzole, a Food and Drug Administration-approved drug for ALS, targets a glutamate transporter, EAAT2, in astrocytes.[15] Thus, development of therapies targeting astrocytes is a subject of intense research.[4,5]

Cellular senescence is characterized by proliferation arrest after extensive cell divisions or upon cellular stresses. The characteristics of cellular senescence include enlarged cell morphology, upregulation of cell cycle inhibitors $p16^{INK4}$ (ref. 16) and $p21^{WAF1}$,[17] senescence-associated β-galactosidase (SA-β-Gal) activity,[18] elevated nitric oxide synthase 2 (NOS2) associated with oxidative stress,[19,20] and DNA double-strand breaks marked by phosphorylated H2AX (γH2AX).[21] Senescent cells secrete various cytokines, growth factors, and proteases that alter tissue microenvironment, which is collectively termed the senescence-associated secretory phenotype (SASP).[22] A major outcome of SASP is tissue inflammation and degeneration mainly through the activity of pro-inflammatory cytokines. In addition to these unfavorable effects, senescent cells and SASP can have beneficial roles in wound healing[23,24] and embryonic development.[25–27]

A main regulator of cellular stress responses and senescence is the *TP53* gene.[28] The human *TP53* encodes, in addition to full-length p53 protein, at least 12 natural protein isoforms through alternative mRNA splicing or alternative promoter usage.[29] Δ133p53, an N-terminal truncated isoform, functions as a negative regulator of cellular senescence by dominant-negatively inhibiting full-length p53.[30,31] p53β, a C-terminal modified isoform, functions as a co-activator of full-length p53 to promote senescence.[30,31]

In this study, we report that Δ133p53 and p53β regulate the neuroprotective and neurotoxic functions of human astrocytes. Using a neuron–astrocyte co-culture system, we demonstrate that downregulation of Δ133p53 or upregulation of p53β in astrocytes promotes SASP and non-cell autonomous neurotoxicity. Furthermore, reconstituted expression of Δ133p53 in neurotoxic astrocytes prevents SASP and reverses them to neuroprotective astrocytes.

Results

Astrocytes express p53 isoforms, Δ133p53 and p53β, and their expression is regulated during cellular senescence. To examine whether p53 isoforms Δ133p53 and p53β are expressed in the human brain, immunofluorescence staining using Δ133p53-specific antibody MAP4 and p53β-specific antibody TLQ40[30,31] was performed in non-disease human brain tissues (Supplementary Table S1). The specificity of the isoform-specific antibodies in immunofluorescence staining was confirmed using a p53-null cell line H358 with a Δ133p53, full-length p53, or p53β expression vector (Supplementary Figures S1A and B). As astrocytes were reported to be a major cell type showing p53 immunoreactivity in non-neoplastic human brain tissues,[32,33] we investigated whether the p53 isoforms would also be expressed in astrocytes and performed co-staining with astrocyte-specific marker glial fibrillary acidic protein (GFAP) (Figure 1a and Supplementary Figure S1C). Both p53β and Δ133p53 signals were detected in GFAP-positive cells and localized within 4′,6-diamidino-2-phenylindole (DAPI)-positive nuclei (Figure 1a and Supplementary Figure S1C, arrows). Nuclei of GFAP-negative cells did not express the isoforms (Figure 1a, arrow heads). These findings indicate that astrocytes are the major cell type in the human brain that express Δ133p53 and p53β.

We examined whether *in vitro* cultured astrocytes also express the p53 isoforms. Primary human astrocytes[34] were serially passaged with monitoring by SA-β-gal staining and $p16^{INK4A}$ (ref. 16) expression (Figures 1b and c) and those at early passage (passage number 5) and approaching senescence (passage number 13) were examined in western blot analysis (Figure 1c; Supplementary Figures S1D and E). Full-length p53 was upregulated during senescence. The Δ133p53-specific antibody detected a single band of 35 kDa corresponding to Δ133p53α[35] (simply called Δ133p53 in this manuscript) in early-passage astrocytes, which was diminished upon senescence. In contrast, p53β (47 kDa) was also upregulated upon senescence. These results indicate that human astrocytes express the p53 isoforms, Δ133p53 and p53β, whose expression profile at cellular senescence is conserved across different cell types.[30,31]

Autophagic degradation of Δ133p53 and SRSF3-mediated regulation of p53β in human astrocytes. To investigate whether increased p53β protein and decreased Δ133p53 protein in senescent astrocytes are due to regulation at the mRNA level, we performed qRT-PCR using RNA samples extracted from serially passaged astrocytes *in vitro* (passage numbers 5 and 13, as above). Similar levels of Δ133p53 mRNA were expressed at both passage numbers (Figure 2a). p53β, by contrast, significantly increased at the mRNA level in astrocytes approaching senescence (Figure 2a). These data indicate that Δ133p53 expression is mainly regulated at the protein level, whereas p53β is regulated at the mRNA level, as we previously reported in human fibroblasts and $CD8^+$ T-lymphocytes.[30,31]

We tested whether Δ133p53 is degraded via selective autophagy in astrocytes, as we had previously reported in senescent fibroblasts and $CD8^+$ T-lymphocytes.[31,36] Senescent astrocytes (passage number 15) with low levels of Δ133p53 were treated with a pharmacological inhibitor of autophagy, bafilomycin A1,[37] whose action was confirmed by increased LC3-II[38] (Figure 2b). Treatment with bafilomycin A1 resulted in the upregulation of Δ133p53 in senescent astrocytes (Figure 2b), suggesting that autophagic degradation of Δ133p53 contributes to its downregulation in these cells. The stabilization of Δ133p53 by bafilomycin A1 was also observed in an immortalized human astrocyte cell line[39,40] (Supplementary Figure S2A). Knockdown of p62/SQSTM1, which is a ubiquitin-binding adaptor specifically functioning in the selective autophagy pathway,[41] also stabilized Δ133p53 (Figure 2c), further supporting the degradation of Δ133p53 via selective autophagy. In addition, whereas proteasome inhibitor MG132 stabilized full-length p53, Δ133p53 was not stabilized but rather decreased in astrocytes (Supplementary Figure S2B), as previously observed in fibroblasts,[30] likely because of induction of autophagy by proteasome inhibition.[42,43] As a splicing factor SRSF3 inhibits the

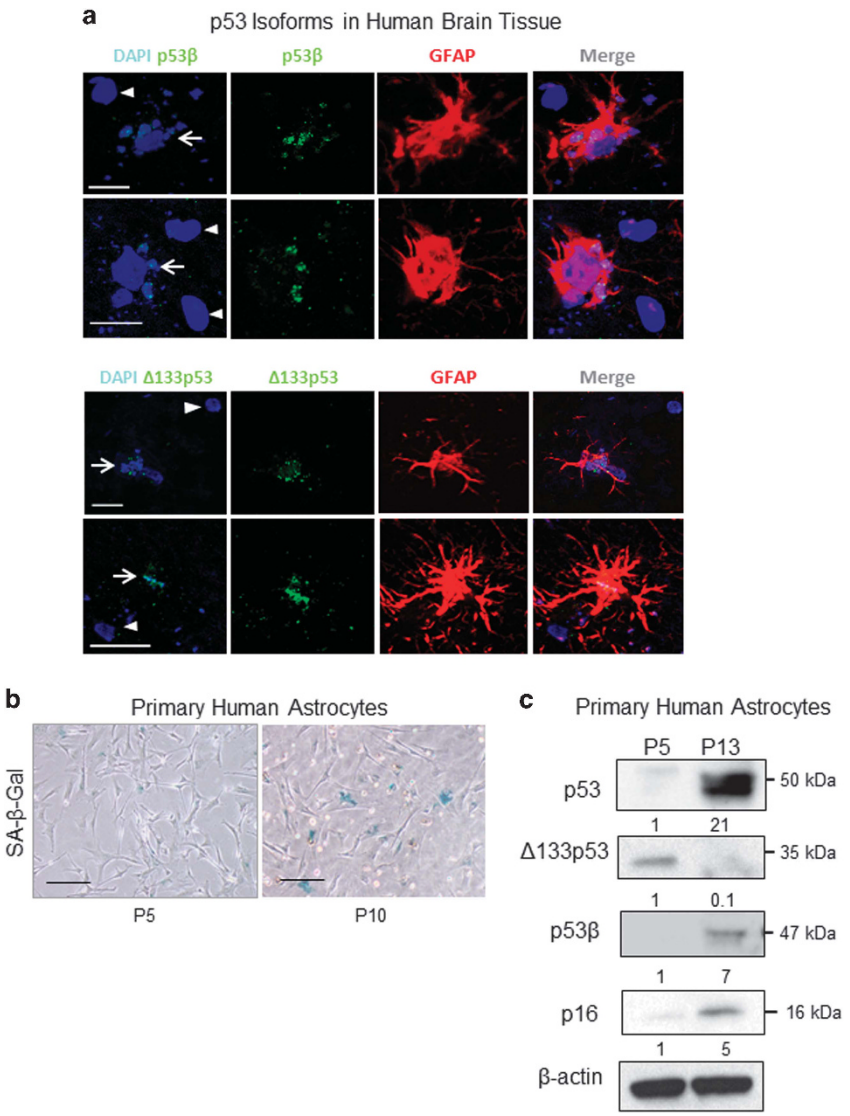

Figure 1 Astrocytes express p53 isoforms, Δ133p53 and p53β, and their expression is regulated during cellular senescence. (**a**) Immunofluorescence staining showing p53β and Δ133p53 expression in GFAP-positive astrocytes (arrows). No expression of p53β and Δ133p53 was observed in GFAP-negative cells (arrow heads). Top panel, non-disease (ND) tissue case 1; bottom panel, ND case 2. Scale bars = 10 μm. (**b**) SA-β-gal staining in primary human astrocytes at passage number 5 (P5) and P10. These astrocytes became completely growth-arrested at P15. Scale bars = 20 μm. (**c**) Western blot analysis of full-length p53, p53 isoforms, and senescence marker $p16^{INK4A}$ in early-passage (P5) and aged (P13) primary human astrocytes. Densitometric values are normalized to β-actin

alternative mRNA splicing generating p53β in human fibroblasts and $CD8^+$ T-lymphocytes,[31,44] we examined whether SRSF3 regulates p53β in astrocytes as well. Knockdown of SRSF3 through small interfering RNA (siRNA) in immortalized astrocytes resulted in a significant increase in p53β mRNA (Figure 2d), consistent with its negative regulation of p53β at the transcript level. These results indicate that the regulatory mechanisms for p53 isoform expression (autophagic degradation of Δ133p53 and SRSF3-mediated regulation of p53β splicing) are conserved in different cell types.

Δ133p53 knockdown or p53β overexpression induces cellular senescence and SASP in human astrocytes. We first recapitulated the senescence-associated expression signature (decreased Δ133p53 and increased p53β) in early-passage primary or immortalized human astrocytes to determine whether it induces these cells to senescence. Immortalized astrocytes were transfected with siRNA specifically targeting Δ133p53[45] or scramble siRNA control, followed by western blot analysis and immunofluorescence staining confirming Δ133p53 knockdown using Δ133p53-specific antibody MAP4[30,31] (Figures 3a and b; Supplementary Figure S3A). Three days following Δ133p53 knockdown, cells became growth-arrested (Figure 3c, top panel) with vacuolization (Figure 3c, bottom panel) and increased SA-β-gal staining (Figures 3d and e), which are characteristics of cellular senescence. Increased mRNA expression of pro-inflammatory cytokines IL-6 and IL-1β, as well as $p21^{WAF1}$, was also observed in these senescent cells (Figure 3f), suggesting that loss of Δ133p53 induces SASP.

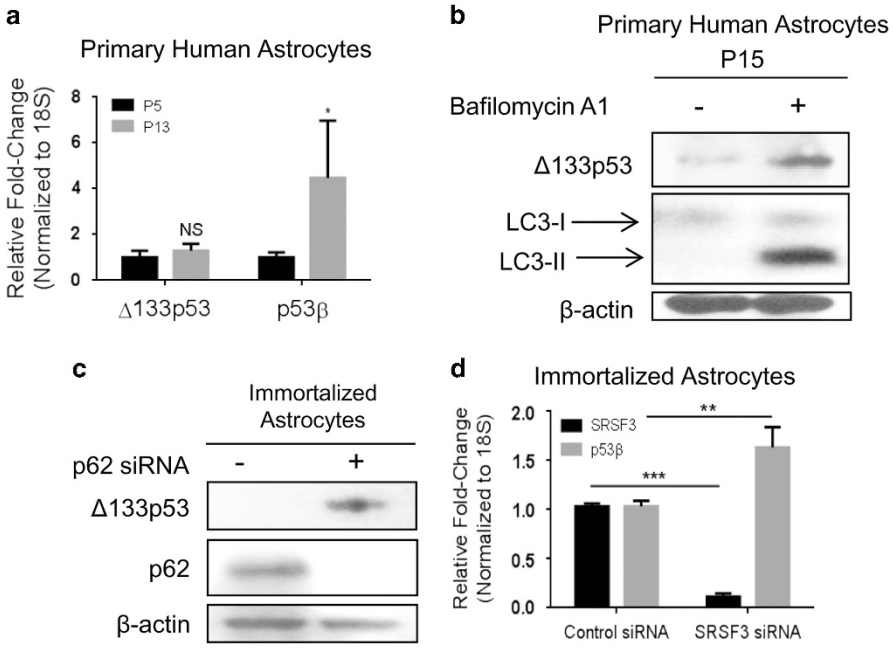

Figure 2 Autophagic degradation of Δ133p53 and SRSF3-mediated regulation of p53*β*. (**a**) qRT-PCR analysis of Δ133p53 and p53*β* in early-passage (P5) and aged (P13) primary astrocytes. (**b**) Δ133p53 expression is restored by bafilomycin A1 treatment (100 nM for 4 h) in senescent human astrocytes (P15). The activity of bafilomycin A1 was confirmed by increased LC3-II. (**c**) Knockdown of p62/SQSTM1 stabilizes Δ133p53. Immortalized astrocytes were transfected with p62/SQSTM1 siRNA (+) or control siRNA (−). (**d**) SRSF3 knockdown induces p53*β* mRNA. Immortalized astrocytes were transfected with SRSF3 siRNA or control siRNA and examined by qRT-PCR for SRSF3 and p53*β* expression. Immortalized astrocytes, which can be transfected with siRNA at a higher efficiency than primary astrocytes, were used in **c** and **d**. Data are presented as mean ± S.E.M. NS indicates $P > 0.05$, $^{*}P \leq 0.05$, $^{**}P \leq 0.01$, $^{***}P \leq 0.001$ by unpaired two-tailed Student's *t* test

Knockdown of Δ133p53 in early-passage primary astrocytes (confirmed by immunofluorescence; Supplementary Figure S3B) also resulted in increased SA-*β*-gal staining (Supplementary Figures S3C and D), the induction of SASP cytokines (Supplementary Figure S3E), and $p21^{WAF1}$ protein expression (Supplementary Figure S3F).

A lentiviral vector driving p53*β* expression or a vector control was transduced to immortalized astrocytes and its overexpression was confirmed by western blot analysis using a p53*β*-specific antibody[30,31] (Figure 4a; Supplementary Figure S4A). Similar to Δ133p53 knockdown, p53*β* overexpression inhibited cell proliferation (Figure 4b), increased SA-*β*-gal-positive cells (Figures 4c and d), and induced pro-inflammatory SASP cytokines IL-6, IL-8, IL-1*β*, and $p21^{WAF1}$ (Figure 4e). Early-passage primary astrocytes with p53*β* overexpression (Supplementary Figure S4B) were also growth-inhibited (Supplementary Figure S4C), had increased SA-*β*-gal staining (Supplementary Figure S4D-E), and induction of SASP (Supplementary Figure S4F). As p53*β* has been shown to promote apoptosis and senescence by differentially regulating gene expression in different cell types,[29,46,47] cell viability as well as expression of Bax, $p16^{INK4}$, and p21 was also assessed (Supplementary Figures S4G-I). Percent cell viability was not significantly affected by overexpression of p53*β* (Supplementary Figure S4G). Consistently, there was no difference in expression of the apoptosis regulator Bax (Supplementary Figure S4H). In contrast, p21 and p16 expression were increased following p53*β* overexpression (Supplementary Figures S4H and I). These results indicate that Δ133p53 downregulation and p53*β* upregulation have causative roles in inducing cellular senescence and SASP in astrocytes.

Increased neuronal death upon co-culture with Δ133p53-knocked-down or p53*β*-overexpressing astrocytes. To examine whether a phenotypic change in astrocytes (such as cellular senescence and SASP via Δ133p53 knockdown or p53*β* overexpression) alters astrocyte-to-neuron interaction, we utilized a co-culture system in which human primary astrocytes were co-plated with induced pluripotent stem cell (iPSC)-derived mature neurons,[48] followed by assays for neuronal survival and death (Supplementary Figures S5A and B). Mature neurons were derived from iPSC (Supplementary Figure S5C) and confirmation of neuronal phenotypes was achieved through expression of sequential markers of differentiation: iPSCs expressed TRA-1-81 demonstrating pluripotency (Supplementary Figure S5D); neural stem cells (NSC) expressed Nestin and Sox1 (Supplementary Figure S5E); and neurons expressed neuronal nuclei marker (NeuN) (Supplementary Figure S5F). Motor neurons, a mature neuronal subtype that is primarily lost in ALS, were also derived from iPSC[49] and their differentiation was confirmed by expression of non-phosphorylated neurofilament marker, SMI-32 (Supplementary Figure S5G).

When early-passage astrocytes with Δ133p53 siRNA or control siRNA (same cells as used in Supplementary Figure S3) were co-cultured with motor neurons for 48 h, Δ133p53-knocked-down, senescent astrocytes induced a higher number of neurons positive for cleaved caspase-3

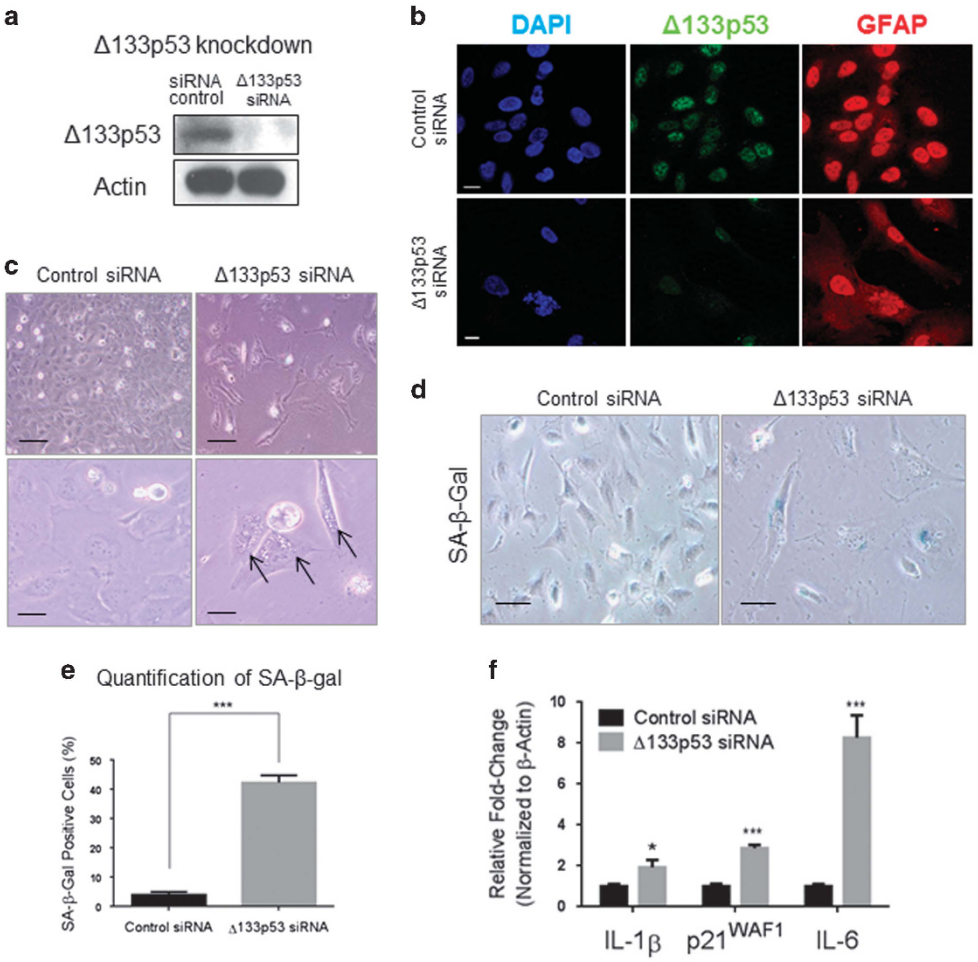

Figure 3 Knockdown of Δ133p53 induces senescent phenotype in astrocytes. Immortalized astrocytes were transfected with Δ133p53 siRNA or control siRNA and analyzed after 3 days. (**a, b**) Confirmation of Δ133p53 knockdown by western blot (**a**) and immunofluorescence (**b**). Scale bars = 10 μm. (**c**) Phase-contrast images of siRNA-transfected astrocytes (upper panel, ×20 magnification; lower panel, ×40 magnification). Arrows show vacuolization. Scale bars = 20 μm. (**d, e**) An increase in SA-β-gal staining by Δ133p53 knockdown. Representative images, scale bars = 20 μm (**d**) and quantitative summary from triplicated experiments (**e**). (**f**) Increase in IL-6, IL-1β, and p21^{WAF1} mRNA expression by Δ133p53 knockdown. qRT-PCR was performed in triplicate. Data are presented as mean ± S.E.M. $^{*}P \leq 0.05$, $^{***}P \leq 0.001$ by unpaired two-tailed Student's *t* test

(15.0 ± 0.2%), a final effector of neuronal apoptosis,[50] than control astrocytes (1.3 ± 0.3%) (Figures 5a and b). Similarly, p53β-overexpressing astrocytes (same cells as used in Supplementary Figure S4) also resulted in an increase in cleaved caspase-3-positive motor neurons (18.8 ± 1.0%) compared with vector control-transduced cells (0.4 ± 0.3%) (Figures 5c and d). To examine the effects of astrocytes on neurons in general and to obtain another quantitative measure, the co-culture experiment was performed using less specialized neurons (generated as in Supplementary Figure S5C) and the number of surviving neurons (NeuN-positive) was counted after 48-h co-culture with astrocytes. A significant decrease in the number of surviving neurons was observed following co-culture with Δ133p53-knocked-down astrocytes (Figures 5e and f) or p53β-overexpressing astrocytes (Figures 5g and h). An increase in neuronal apoptosis by p53β-overexpressing astrocytes was also confirmed in this experimental setting (Supplementary Figures S5H and I). These findings indicate that the senescence-associated p53 isoform expression signature confers astrocytes with neurotoxic activity.

Δ133p53 protects astrocytes from senescence and enhances their neuroprotective function. The induction of astrocyte senescence and neurotoxicity by reproducing the senescence-associated p53 isoform expression signature (Figures 3, 4, and 5) prompted us to hypothesize that manipulated expression of the p53 isoforms (which in this case recapitulates the expression profile in early-passage astrocytes) may also lead to senescence inhibition and neuroprotective function in astrocytes. To test this hypothesis, Δ133p53 expression was reconstituted via lentiviral vector transduction in primary astrocytes approaching senescence (passage number 12) (Figure 6a). Reconstituted expression of Δ133p53 restored cell proliferation (Figure 6b), decreased SA-β-gal-positive cells (Figures 6b and c), and reduced the levels of pro-inflammatory SASP cytokines IL-6 and IL-1β (Figure 6d). Significantly, two neurotrophic growth factors, NGF and IGF-1, out of the three examined were two to

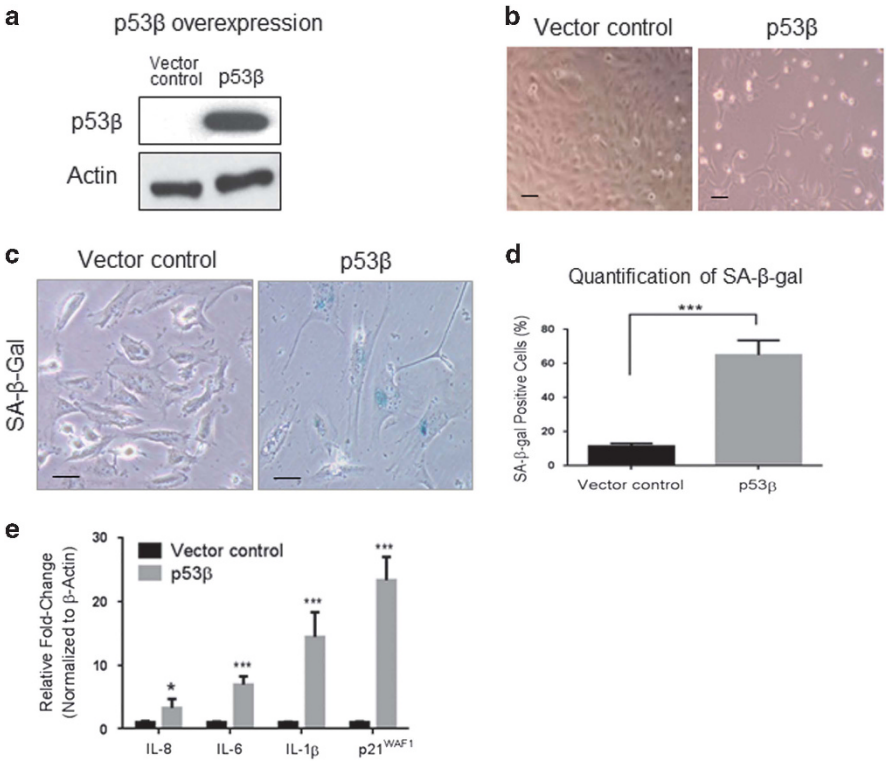

Figure 4 Overexpression of p53β induces senescent phenotype in astrocytes. Immortalized astrocytes were transduced with p53β lentiviral vector or control vector and analyzed after 3 days. (**a**) Confirmation of p53β overexpression by western blot. (**b**) Phase-contrast images of transduced astrocytes. Scale bars = 20 μm. (**c, d**) An increase in SA-β-gal staining by p53β overexpression. Representative images, scale bars = 20 μm (**c**) and quantitative summary from triplicated experiments (**d**). (**e**) Elevated mRNA expression of IL-8, IL-6, IL-1β, and p21^{WAF1} by p53β overexpression. qRT-PCR was performed in triplicate. Data are presented as mean ± S.E.M. *$P \leq 0.05$, ***$P \leq 0.001$ by unpaired two-tailed Student's *t* test

threefold upregulated by Δ133p53 reconstitution (Figure 6d). Immunofluorescence staining of NGF confirmed its increased expression in Δ133p53-reconstituted astrocytes (Supplementary Figure S6A), which was comparable with that in early-passage astrocytes (Supplementary Figure S6B).

We then used these Δ133p53-reconstituted astrocytes in the co-culture experiment (as performed in Figure 5). Vector control-transduced astrocytes (derived from passage number 12) resulted in a much larger number of motor neurons positive for cleaved caspase-3 (35.0 ± 2.0%; Figures 6e and f) than those derived from passage number 5 (1.3 ± 0.3%; Figures 5a–d), indicating a senescence-associated progression of neurotoxicity in astrocytes. The reconstitution of Δ133p53 in these near-senescent astrocytes significantly reduced the number of cleaved caspase-3-positive motor neurons (~12%; Figures 6e and f), suggesting that Δ133p53 in astrocytes functions to suppress neuronal apoptosis. Counting of NeuN-positive neurons following co-culture (Figures 6g and h) also showed that aged astrocytes were less neuroprotective than early-passage astrocytes (compare controls in Figure 6h *versus* Figures 5f and h), and that reconstituted expression of Δ133p53 restored the number of surviving neurons back to the level exerted by early-passage astrocytes (Δ133p53 in Figure 6h; compare with controls in Figures 5f and h).

To confirm the roles of NGF and IL-6 in Δ133p53-mediated astrocyte neuroprotective and neurotoxic function, neutralizing antibodies were used in co-culture experiments. As a positive control for IL-6-neutralizing antibody, we first performed immunofluorescence staining of untreated neurons and neurons treated with IL-6 alone or both IL-6 and IL-6-neutralizing antibody (IL-6-NAb). Cleaved caspase-3 immunofluorescence staining was increased upon IL-6 treatment and reduced back to the control level upon co-incubation with IL-6-NAb (Supplementary Figure S6C). Consistently, the number of NeuN-positive surviving neurons was significantly reduced upon IL-6 treatment and restored by IL-6-NAb (Supplementary Figures S6C and D). These results confirmed that IL-6 promotes neurotoxicity and that IL-6-NAb is effective at neutralizing its function. Next, we used IL-6-NAb in co-culture experiments with neurons and aged astrocytes (P12) (Figure 6i, Supplementary Figure S6E). In these co-culture experiments, incubation with IL-6-NAb reduced neuronal apoptosis (indicated by cleaved caspase-3-positive neurons) to the level of Δ133p53-reconstituted astrocytes, but there was no combinatorial effect of Δ133p53 and IL-6-NAb over either alone (Figure 6i, Supplementary Figure S6E). In co-culture experiments with NGF-neutralizing antibody (NGF-NAb), the reduction in neuronal apoptosis by Δ133p53 reconstitution was abolished by NGF-NAb, and thus the level of neuronal apoptosis in Δ133p53-reconstited astrocytes with NGF-NAb was similar to that in control astrocytes with or without NGF-NAb (Figure 6i, Supplementary Figure S6E). These results indicate that Δ133p53 in astrocytes promotes

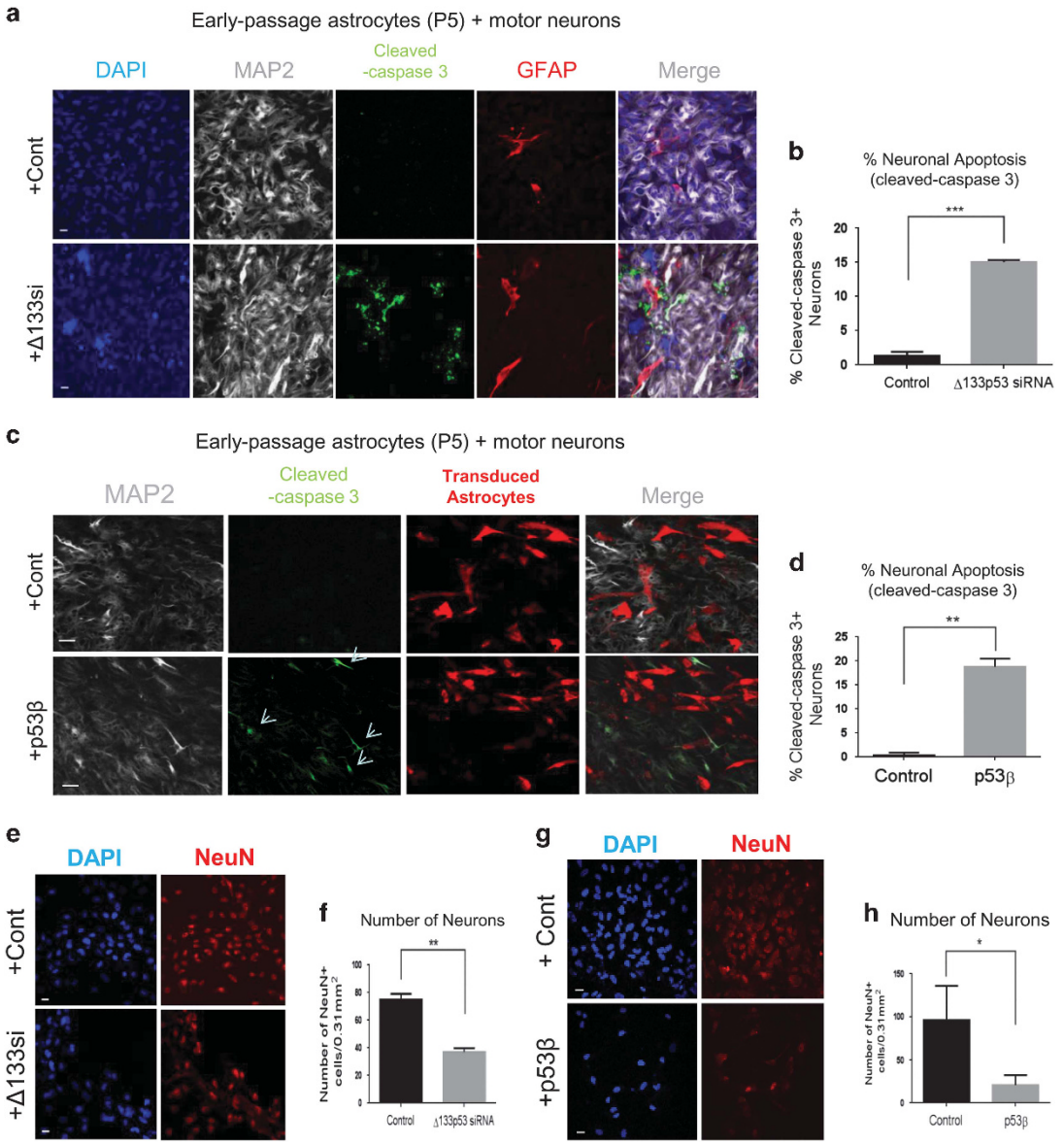

Figure 5 Increased neuronal death upon co-culture with Δ133p53-knocked-down or p53β-overexpressing astrocytes. Early-passage primary astrocytes (P5) with Δ133p53 siRNA and control siRNA (generated as in Supplementary Figure S3) (**a, b, e,** and **f**) and those with p53β -overexpression or control vector (generated as in Supplementary Figure S4) (**c, d, g,** and **h**) were used in co-culture for 48 h with motor neurons[49] or less specialized neurons (as generated as in Supplementary Figures S5C-F). (**a** and **c**) Immunofluorescence staining of MAP2 (neuronal marker) and cleaved caspase-3 (apoptosis marker). Astrocytes are marked by GFAP (**a**) or fluorescent signals derived from the lentiviral vectors (**c**). Scale bars = 10 μm. (**b** and **d**) Quantification of neuronal apoptosis. Cleaved caspase-3-positive neurons per total number of MAP2-positive neurons were counted in triplicate experiments in five microscopic fields (×40 magnification). (**e** and **g**) Immunofluorescence staining of NeuN (neuronal marker). Scale bars = 10 μm. (**f** and **h**) Quantification of number of neurons. Total number of NeuN-positive neurons were counted in at least five microscopic fields (×40 magnification) in triplicate experiments. Data are presented as mean ± S.E.M. $^*P \leq 0.05$, $^{**}P \leq 0.01$, $^{***}P \leq 0.001$ by unpaired two-tailed Student's *t* test

neuroprotection through upregulation of NGF and down-regulation of IL-6.

Increased senescent astrocytes in brain tissues from neurodegenerative disease patients. To examine whether neurodegenerative disease tissues have increased features of cellular senescence, AD, ALS, age-matched non-disease, and non-disease pediatric tissues (Supplementary Table S1) were obtained. Immunohistochemical staining was performed using antibodies to proteins known to be associated with cellular senescence, such as $p16^{INK4A}$,[16] NOS2,[20] and γH2AX[21] (Figure 7a). An increase in the senescence-associated biomarkers was prominent in all neurodegenerative samples examined compared with controls (Figure 7a). Quantification of the number of $p16^{INK4A}$-expressing cells revealed a significant increase in this senescence-associated gene in AD and ALS tissues (Figure 7b). Although both AD and ALS are associated with increased cellular senescence, qRT-PCR using brain tissue RNA samples showed that SASP cytokine IL-6 and a p53-inducible senescence

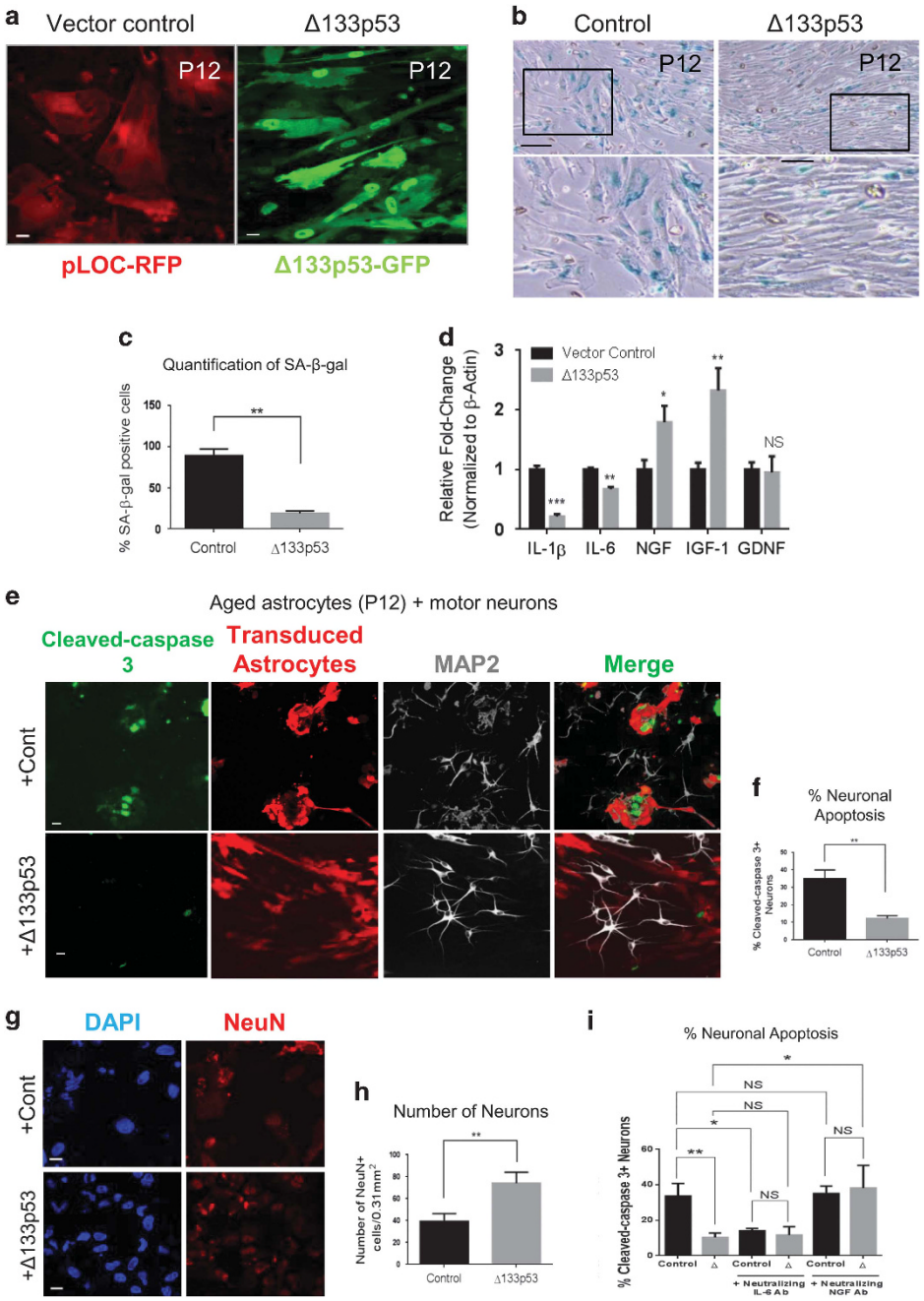

Figure 6 Δ133p53 protects astrocytes from senescence and enhances neuroprotective function. Aged primary astrocytes (P12) were transduced with a lentiviral vector driving Δ133p53 or its control vector and analyzed after 3 days. (**a**) Confirmation of lentiviral transduction by RFP (vector control) or GFP (Δ133p53). Scale bars = 10 μm. (**b**) Decreased SA-β-gal staining by reconstituted expression of Δ133p53. Representative images of SA-β-gal staining (top panels, scale bars = 20 μm) and enlarged images of the insets (bottom panels). (**c**) Quantitative summary of SA-β-gal staining from triplicated experiments. (**d**) Decreased expression of IL-1β and IL-6 and increased expression of NGF and IGF-1. qRT-PCR analysis was performed in triplicate. (**e–h**) Δ133p53-reconstituted astrocytes and control astrocytes were used in co-culture with motor neurons (**e** and **f**) or less specialized neurons (**g** and **h**), as performed in Figure 5. (**e**) Decrease in cleaved caspse-3-positive motor neurons upon co-culture with Δ133p53-reconstituted aged (P12) astrocytes. Immunofluorescence staining of cleaved caspase-3 and MAP2 was performed. Astrocytes were detected by the vector-derived fluorescence. Scale bars = 10 μm. (**f**) Quantification of neuronal apoptosis. Data were achieved by counting the number of cleaved caspase-3-positive neurons per total number of MAP2-positive neurons in triplicate experiments in five microscopic fields (×40 magnification). (**g**) Immunofluorescence staining of NeuN. Scale bars = 10 μm. (**h**) Quantification of number of NeuN-positive neurons. Total number of NeuN-positive neurons were counted in at least five microscopic fields (×40 magnification) in triplicate experiments. (**i**) Quantification of neuronal apoptosis in co-culture experiments with IL-6 or NGF-neutralizing antibodies. Data were from the experiment shown in Supplementary Figure S6E and achieved by counting the number of cleaved caspase-3-positive neurons per total number of NeuN-positive neurons in triplicate experiments in five microscopic fields (×40 magnification). Data are presented as mean ± S.E.M. NS indicates $P > 0.05$, $^{*}P \leq 0.05$, $^{**}P \leq 0.01$, $^{***}P \leq 0.001$ by unpaired two-tailed Student's *t* test

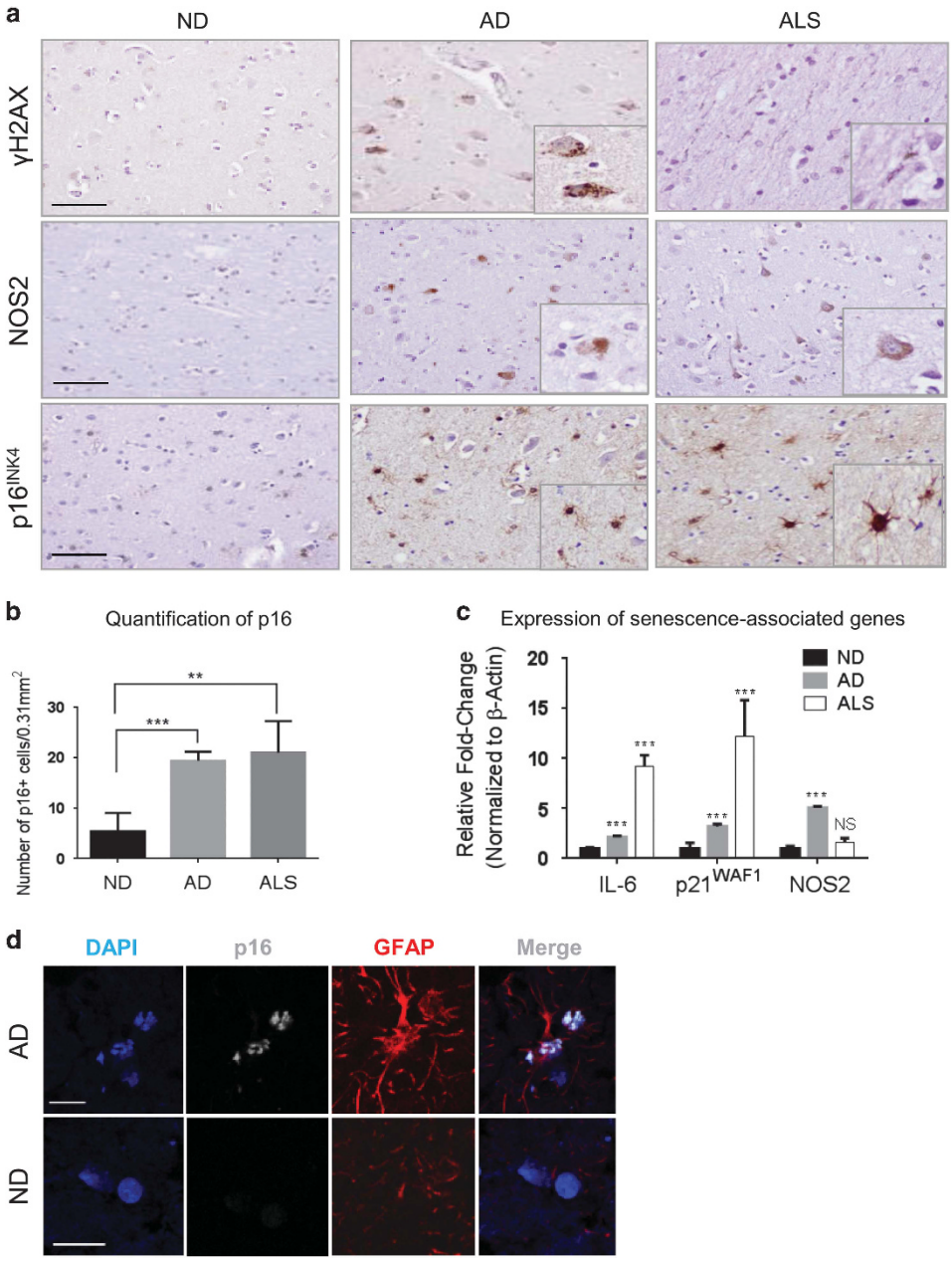

Figure 7 Increased senescent astrocytes in brain tissues from neurodegenerative disease patients. (**a**) Increased expression of senescence-associated proteins, γH2AX, NOS2, and p16INK4A, in AD (case 5), and ALS (case 4). Non-disease (ND) age-matched control tissue was case 5. Scale bars = 50 μm. Insets in AD and ALS show enlarged positive cells. (**b**) Quantification of p16INK4A-positive cells in AD (cases 1–4) and ALS (cases 1–3) compared with ND (cases 1–4). (**c**) Elevated mRNA expression of senescence-associated genes in AD (cases 1–4) and ALS (cases 1–3) compared to ND (cases 1–4). qRT-PCR experiments were performed in triplicate. Data are presented as mean ± S.E.M. (**d**) Increase in p16INK4A- and GFAP-positive cells in AD (case 1) compared to ND (case 1). Scale bars = 10 μm. NS indicates $P > 0.05$, $^{**}P \leq 0.01$, $^{***}P \leq 0.001$ by unpaired two-tailed Student's *t* test

regulator $p21^{WAF1}$ were upregulated more remarkably in ALS, while NOS2 upregulation was more evident in AD (Figure 7c), possibly reflecting the different disease pathologies. IL-6 and $p21^{WAF1}$ expression levels were much lower in pediatric brain tissues *versus* aged brain tissues (Supplementary Figure S7A), indicating that these senescent changes not only are associated with neurodegenerative diseases, but also may occur during physiological brain aging. In agreement with astrocyte-like morphology of the senescent cells (Figure 7a), immunofluorescence co-staining of $p16^{INK4A}$ and GFAP as an astrocyte marker showed that the senescent cells were astrocytes (Figure 7d). Furthermore, both immunohistochemical (Supplementary Figure S7B) and immunofluorescence staining (Supplementary Figure S7C) of GFAP showed the presence of astrocytes with enlarged and flattened cytoplasms, which is characteristic of senescent cells,[51] in AD and ALS brain tissues, but not in non-disease control tissues.

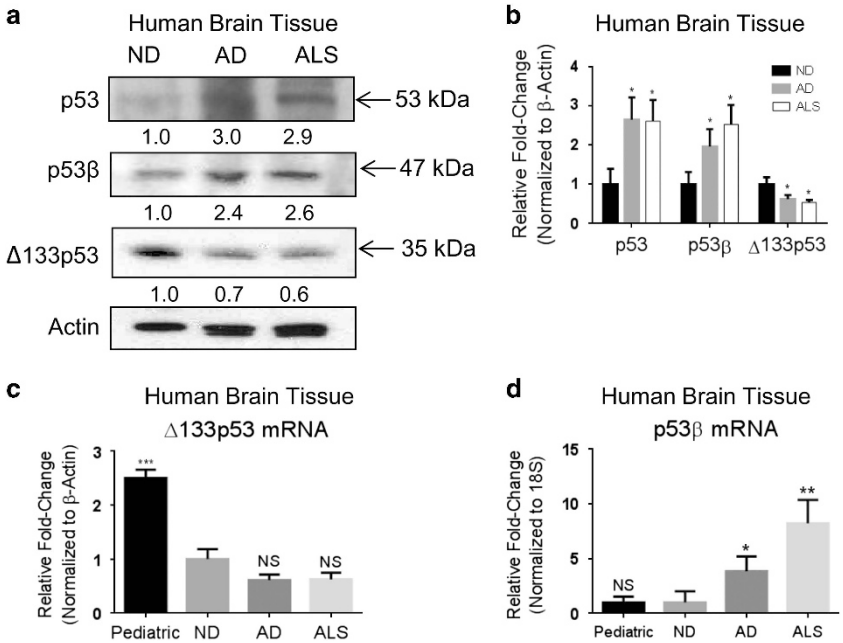

Figure 8 p53*β* is upregulated and Δ133p53 is downregulated in neurodegenerative diseases. (**a**) Representative western blot showing elevated expression of full-length p53 and p53*β* and decreased Δ133p53 expression in AD (case 3) and ALS (case 3) compared with non-disease (ND) age-matched control brain tissue (case 2). Densitometric values are normalized to *β*-actin. (**b**) Summary of densitometric analyses of western blots from AD (cases 1–4), ALS (cases 1–3), and ND (cases 1–4). (**c** and **d**) qRT-PCR analysis of Δ133p53 (**c**) and p53*β* (**d**) in pediatric brain tissue (cases 1–4), ND control (cases 1–4), AD (cases 1–4), and ALS (cases 1–3). Expression levels are shown relative to ND. Densitometric values are normalized to *β*-actin. Data are presented as mean ± S.E.M. $^{*}P \leq 0.05$, $^{**}P \leq 0.01$, $^{***}P \leq 0.001$ by unpaired two-tailed Student's *t* test

p53*β* is upregulated and Δ133p53 is downregulated in neurodegenerative disease brains. To examine the expression of p53*β* and Δ133p53 in AD, ALS, and age-matched non-disease brain tissues, western blot analysis was performed using the Δ133p53-specific antibody MAP4 and the p53*β*-specific antibody TLQ40,[30,31] along with detection of full-length p53. Only the 35 kDa Δ133p53 bands corresponding to Δ133p53*α*, but not smaller-size bands corresponding to Δ133p53*β* and Δ133p53*γ*, were detected by MAP4 in these brain tissues (Supplementary Figure S8A). The major bands detected by TLQ40 were 47 kDa in size, which corresponds to p53*β* that starts at the same methionine as full-length p53, with smaller amounts of N-terminally truncated *β* isoforms (Supplementary Figure S8B). These detection patterns are similar to those observed in primary human astrocytes (Figure 1c). We found that full-length p53 (53 kDa) and p53*β* (47 kDa) were upregulated, whereas Δ133p53 (35 kDa) was downregulated, in AD and ALS tissues compared with non-disease tissues (Figure 8a). Quantitative densitometric analysis determined that the upregulation of full-length p53 and p53*β* was two to threefold and the downregulation of Δ133p53 was 0.5–0.6-fold (Figure 8b). The upregulation of p53*β* and the downregulation of Δ133p53 in neurodegenerative diseases are consistent with the expression profiles of these p53 isoforms observed in senescent astrocytes *in vitro* (Figure 1c), as well as other *in vivo* conditions associated with increased senescence, such as pre-malignant colon adenomas[30] and $CD8^+$ T-lymphocytes in the elderly.[31] The expression levels of Δ133p53 mRNA were not significantly changed between non-disease and AD or ALS tissues (Figure 8c), while p53*β* mRNA was increased in AD and ALS compared with non-disease tissues (Figure 8d), again in agreement with the observations in senescent astrocytes *in vitro* (Figure 2a) and $CD8^+$ T-lymphocytes *in vivo*.[31] A higher level of expression of Δ133p53 mRNA in non-disease pediatric tissues compared with non-disease aged brain tissues (Figure 8c) may also suggest a transcriptional control of Δ133p53 during physiological brain development and aging. Thus, AD and ALS are associated with increased astrocyte senescence and the senescence-associated p53 isoform expression signature, validating that our *in vitro* experiments using serially passaged human astrocytes recapitulate part of *in vivo* pathology of these neurodegenerative diseases.

Discussion

Astrocytes exert both neuroprotective and neurodegenerative effects in a context-dependent manner, which are associated with either repression or induction of SASP, respectively.[52] The data are consistent with the notion that the astrocyte-mediated effects of the p53 isoforms on neurons are exerted through their regulatory roles for SASP (Figures 3f, 4e, and 6d and i, Supplementary Figure S6E). One main feature of astrocyte SASP driving neuronal loss is the release of pro-inflammatory cytokines such as IL-6.[53] Consistent with the neurodegenerative role of these SASP cytokines, the induction of SASP in astrocytes either by Δ133p53 knockdown (Figure 3f) or by p53*β* overexpression (Figure 4e) leads to increased neuronal apoptosis (Figures 5a–d), while the repression of astrocyte SASP by Δ133p53 restoration (Figure 6d) leads to increased neuronal survival (Figures 6e and f). Our data suggest that IL-6 is a therapeutic target in astrocytes to prevent neurotoxicity (Figure 9b).

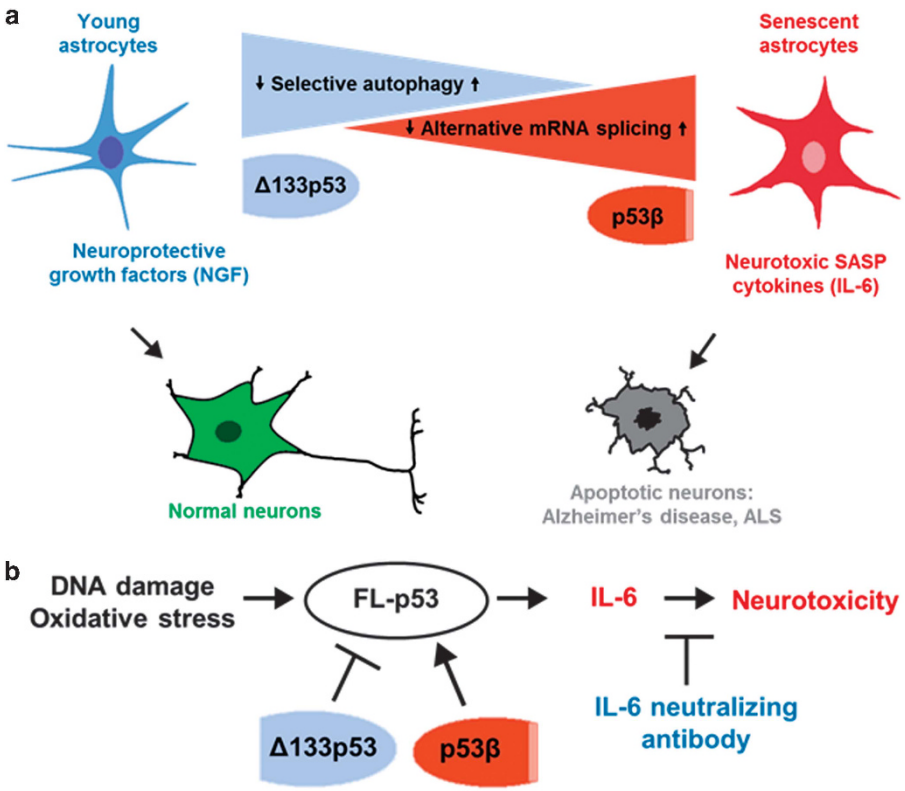

Figure 9 Proposed models of the p53 isoform regulation of astrocyte-mediated neuroprotection and neurodegeneration. (**a**) The p53 isoforms regulate astrocyte-mediated neuroprotection and neurodegeneration. Δ133p53, which is regulated by selective autophagy-mediated degradation,[36] is abundant in early-passage astrocytes *in vitro* and astrocytes in non-disease brain tissues (here collectively termed 'young') and contributes to the neuroprotective function of these 'young' astrocytes. p53*β*, which is generated via alternative mRNA splicing,[44] is induced in senescent astrocytes *in vitro* and in neurodegenerative disease brain tissues and contributes to the neurotoxic effect of these senescent astrocytes. (**b**) IL-6 is a therapeutic target in astrocytes to prevent neurotoxicity. DNA damage and oxidative stress activate full-length p53 (FL-p53), which leads to transcriptional activation of IL-6[57] and neurotoxicity. The modulation of FL-p53 activity by the p53 isoforms, as well as IL-6-neutralizing antibody, prevents neurotoxicity

The data also indicate that the upregulation of neurotrophic growth factors such as NGF and IGF-1 in astrocytes (Figure 6d, Supplementary Figure S6A) mediates Δ133p53-induced neuroprotection (Figures 6g–i, Supplementary Figure S6E). NGF and IGF-1 are known to promote neuronal survival[54,55] and are decreased in Alzheimer's and Parkinson's disease brain tissues.[11,12] Furthermore, astrocytes utilize IGF-1 to protect neurons from oxidative stress.[56] Although this study focused on astrocyte-to-neuron signaling, possible roles of the p53 isoforms in neurons and neuron-to-astrocyte signaling in neurodegenerative disease deserve further investigation.

Full-length p53 is known to transactivate pro-inflammatory cytokine genes such as IL-6 and IL-8.[57] It is thus likely that the effect of p53*β* or Δ133p53 on SASP and neurodegeneration is at least in part through cooperation with or dominant-negative inhibition of full-length p53.[30,31] As full-length p53 functions to inhibit the IGF-1 signaling pathway,[58] the dominant-negative inhibition by Δ133p53 of full-length p53 activity[30] may increase IGF-1 signaling towards neuroprotection. Another possibility is that Δ133p53 may directly upregulate the neurotrophic factors NGF and IGF-1 through its gain-of-function activity, which was recently reported to activate a set of genes for DNA damage repair.[59] Although *in silico* analysis of the NGF and IGF-1 gene promoters did not identify a perfect match to the predicted Δ133p53-binding response element,[59] further studies will elucidate the regulation of these neurotrophic factors by Δ133p53 in dominant-negative and gain-of-function manners.

A phenotypic shift from neurotoxic SASP astrocytes to neuroprotective astrocytes may represent a promising therapeutic approach for inhibiting or delaying the progression of neurodegenerative diseases. In the proposed model (Figure 9), enhancement of Δ133p53 activity and/or inhibition of p53*β* activity could lead to such phenotypic shift of astrocytes. Because increased neurotoxicity, which was exerted by *in vitro* aged astrocytes and reverted by reconstituted expression of Δ133p53 in this study, is also characteristic of astrocytes derived from patients with neurodegenerative diseases,[60,61] our findings have implications in developing therapeutic interventions. This study provides a rationale for exploration of small molecules that can modulate the expression level or activity of the p53 isoforms to inhibit the progression of neurodegeneration. Finally, only humans and other primates have the equivalent of Δ133p53 (Supplementary Figure S9). It is interesting whether this primate-specificity of Δ133p53 is related to primate-specific accumulation of *β*-amyloid[62] and other physiological or pathological processes specific or preferential to humans and other primates.

Materials and Methods

Primary cells and cell lines. Primary human astrocytes were obtained from Sciencell (Carlsbad, CA, USA).[34] They were maintained in Astrocyte Medium supplemented with 2% fetal bovine serum, 1% astrocyte growth supplement from Sciencell, and 1% penicillin/streptomycin solution. When confluent, cells were split at a ratio of 1:4 (earlier passages) to 1:2 (later passages) until they reached replicative senescence. For immortalized human astrocytes, human fetal brain material was dissected from 8- to 12-week-old abortuses, aspirated through a 19-gauge needle, washed twice with Eagle's minimum essential medium and plated onto poly-D-lysine (0.1 mg/ml)-coated flasks. After 3 weeks, cells were transfected using calcium phosphate precipitation with a plasmid DNA containing the SV40 mutant with a deletion of its origin of replication (pMK16).[39,40] H358 cells were purchased from American Type Culture Collection (Manassas, VA, USA).

Plasmid constructs. To generate retroviral expression vectors of human p53 isoforms, Flag-tagged p53β was PCR-amplified using pSVp53β and pSVDNp53,[29] respectively, as templates and then inserted into *Not*I and *Eco*RI sites of a pQCXIN vector (BD Biosciences, Franklin Lakes, NJ, USA). These constructs were verified by DNA sequencing. The Precision LentiORF RFP control vector (which drives RFP as an ORF insert, as well as IRES-translated GFP from the pLOC lentiviral vector backbone) was purchased from Open Biosystems/GE Dharmacon (Lafayette, CO, USA). For overexpression of p53β and Δ133p53, the RFP insert was replaced with cDNA inserts of p53β and Δ133p53, respectively.

Retroviral and lentiviral transduction. The retroviral constructs were transfected into Phoenix packaging cells (Orbigen, Inc., San Diego, CA, USA) using Lipofectamine 2000 (Invitrogen, Paisley, Renfrewshire, UK). Lentiviral supernatants were obtained using the Trans-lentiviral packaging system (Open Biosystems). Retro- and lentiviral vector supernatants were collected 48 h after transfection and used to infect cells in the presence of polybrene (8 μg/ml; Sigma–Aldrich, St. Louis, MO, USA). Two days after infection, the cells were selected with G418 (600 μg/ml; Sigma–Aldrich), puromycin (2 μg/ml; Sigma–Aldrich) or zeocin (1 mg/ml; Invitrogen).

Transfection of siRNA oligonucleotides. siRNA oligonucleotides were transfected at a final concentration of 12 nM using Lipofectamine RNAiMAX (Invitrogen). The following oligonucleotides were from Invitrogen Stealth Select siRNA targeting Δ133p53: 5′-GGAGGUGCUUACACAUGUU-3′,[45] p62/SQSTM1: 5′-AGAAGUGGACCCGUCUACAGGUGAA-3′,[36] SRSF3: 5′-AGAGCUAGAUGGAA GAACATT-3′,[44] and Stealth non-specific RNAi negative control (no. 12,935-100).

SA-β-gal staining and cell treatments. SA-β-gal staining was performed with the Senescence-β-Galactosidase Staining Kit (Cell Signaling Technology, Danvers, MA, USA). Bafilomycin A1 was obtained from Sigma–Aldrich and incubated for 4 h at a concentration of 100 nM. MG132 was obtained from LC Laboratories (Woburn, MA, USA) and incubated for 8 h at a concentration of 15μM.

Cell viability assay. Cell pellets were resuspended in 20 ul of Trypan blue and cell viability was calculated using a TC20 Automated Cell Counter (Bio-Rad, Hercules, CA, USA).

Neuronal differentiation of iPSCs. The iPSC line, i20 (NIH stem cell bank), was differentiated to NSCs, and then to neurons using Gibco Pluripotent Stem Cell Neural Induction (Life Technologies, Frederick, MD, USA). For motor neuron differentiation, iPSCs were grown to 80% confluency, then digested with collagenase IV (Invitrogen) for 8 min. Cells were scraped off of the dish, and after settling, the supernatant was aspirated, and cells were re-plated into low adherence dishes (Corning, Corning, NY, USA) in KSR (Invitrogen)-based media with 20 ng/ml FGF (R&D Systems, Minneapolis, MN, USA), 20 μM ROCK-I (Tocris, Bristol, UK), 10 μM SB431542 (Tocris), and 0.2 μM LDN193189 (Stemgent). Embryoid bodies were transitioned to a KSR-free medium after 3 days. Retinoic acid was added to the media after 5 days to direct the cells towards a rostral spinal cord phenotype, with additional patterning using 1 μM smoothened agonist (Calbiochem, Billerica, MA, USA) and 0.5 μM purmorphamine (Stemgent, Cambridge, MA, USA) after 7 days to ventralize the differentiating population. After 14–16 days in suspension, the embryoid bodies were dissociated and plated on dishes coated with polyornithine or poly-D-lysine and laminin for an additional 7–14 days. Neuronal cultures were maintained in neurobasal media (Invitrogen) with 25 μM glutamate (Sigma, St. Louis, MO, USA), 0.4 μg/ml ascorbic acid (Sigma), 10 ng/ml GDNF (Sigma), 10 ng/ml CNTF (Sigma), 1 μg/ml laminin (BD Biosciences). B-27, N2, non-essential amino acids, and pen/strep/glutamine were all from Invitrogen. Two days after plating, 10 nM dihydrotestosterone was added, and the cultures were maintained for an additional 7–14 days.

Co-culture system. Following differentiation of iPSC to NSCs, NSCs were plated at a density of 3×10^4 cells/cm^2 in a four-well chamber slide coated with 20 μg/ml poly-L-ornithine and 10 μg/ml laminin. Media was changed to neural differentiation media (1 × Neurobasal Medium, 2% B-27 Serum-Free Supplement, 2 mM GlutaMAX-1 Supplement, Life Technologies) after 2 days. Media was changed every 3 days and NSCs were allowed to mature neurons for 1 month. Primary human astrocytes were plated on top of the mature neurons at a density of 3×10^4 cells/cm^2. Media was changed to a 1:1 ratio of astrocyte (Sciencell) and neuron differentiation medium.[48,63,64] After 48 h, cells were fixed with 4% paraformaldehyde for immunocytochemistry staining. Percent apoptosis was calculated by counting number of cleaved caspase-3-, MAP2-, or NeuN-positive neurons in triplicate experiments in five microscopic fields (×40 magnification) for three biological replicates. In addition, the number of neurons remaining after the 48 h co-culture period was also quantified with five frames per condition for three biological replicates and counting the number of NeuN-positive neurons.

Recombinant IL-6 and neutralizing antibody treatments. Recombinant IL-6 (Invivogen, San Diego, CA, USA) was incubated for 24 h at a concentration of 5 ng/ml. In experiments with neutralizing antibodies, co-culture was performed as above with NGF neutralizing antibody (Alomone labs, Jerusalem, Israel) at a concentration of 500 ng/ml or IL-6 neutralizing antibody (Invivogen) at a concentration of 5 μg/ml. After 48 h, cells were fixed and stained as described above.

Immunohistochemistry and immunofluorescence. Frozen and formalin-fixed paraffin embedded human tissue sections were washed in PBS before blocking for 1 h in PBS containing 0.1% Triton-X and 10% donkey serum (Sigma–Aldrich). Donkey serum is used to block non-specific binding sites before incubation with primary antibody overnight at 4 °C. Antigens were detected using the antibodies listed in Supplementary Table S2. After overnight incubation, they were washed in PBS three times for 10 min, before incubation with the appropriate conjugated secondary antibodies for 1 h at room temperature. The secondary antibody was conjugated to fluorophores: Alexa-488, -568, and -647 (Invitrogen; 1:400). After washing in PBS three times for 10 min, sections were incubated for 10 min in 4',6-diamidino-2-phenylindole (10ug/ml, Sigma–Aldrich) to counterstain the cell nuclei, and rinsed three times for 10 min in 0.1 M phosphate buffer. Sections were mounted and slides coverslipped with FluorSave mounting medium (Millipore, Billerica, MA, USA). Omission of primary antibody was used as a negative control in all immunofluorescence experiments. For immunohistochemistry on paraffin sections, slides were heated to 65 °C before immersion in histoclear and rehydration with graded alcohols. Sections were blocked in 1% H2O2 in PBS-Tween 20 (PBS-T) and then in 5% normal goat serum in PBS-T. Antigens were detected using the antibodies listed in Supplementary Table S2. Binding of the primary antibody was detected using a biotinylated secondary antibody listed in Supplementary Table S3 with an ABC standard kit (Vector Laboratories, Burlingame, CA, USA). Visualization was enabled using a 0.05% diaminobenzene hydrochloride solution (Sigma–Aldrich). Omission of primary antibody was used as negative controls in all immunohistochemistry experiments.

Immunocytochemistry. Cells were washed with PBS and fixed for 10 min with 4% paraformaldehyde. Cells were permeabilized with 0.01% Triton-X for 4 min, washed with PBS and then blocked in 5% FBS for 1 h at room temperature. Primary antibodies listed in Supplementary Table S2 were applied overnight at 4 °C. Cells were washed with PBS before incubation with a secondary antibody conjugated to fluorophores: Alexa-488, 568- and -647 at a dilution of 1:400 (Life Technologies) and 4',6-diamidino-2-phenylindole for 1 h. Coverslips were mounted on to slides with FluorSave mounting medium (Chemicon). Omission of primary antibody was used as a negative control in all immunocytochemistry experiments.

Immunoblotting. Cells and tissues were lysed in RIPA buffer. Lysates were kept on ice for 30 min prior to sonication. Protein concentration was measured using the Bradford assay method. NuPAGE 4 × loading buffer was added to all lysates and then boiled for 5 min. Then, 40 μg of protein was loaded onto a Tris-glycine gel

(Thermo Scientific, Waltham, MA, USA) for electrophoresis. Proteins were then transferred onto a PVDF membrane. Membranes were blocked in 1:1 mixture of Superblock and Tris-Buffered Saline (TBS, 125 mM Tris and 200 mM NaCl), containing 0.1% Tween-20. Membranes were incubated in the primary antibodies listed in Supplementary Table S2 overnight at 4 °C, and washed three times in TBS-Tween-20. Membranes were then incubated in secondary antibody listed in Supplementary Table S3 for 1 h at room temperature and the signal visualized SuperSignal developing reagent and visualized using X-ray films (Fujifilm, Tokyo, Japan).

RNA extraction and cDNA preparation. mRNA was extracted using the RNeasy Mini Kit (Qiagen, Crawley, UK) according to the manufacturer's instructions. For mouse brain tissue, 10–20 mg of frozen cortical tissue was added to 300 μl lysis buffer containing 0.001% β-mercaptoethanol. Tissues or cells were homogenized and lysate mixed 1:1 with 70% ethanol and centrifuged through an RNeasy Mini Spin column. The column was washed and treated with DNAse 1 for 15 min, before washing again to remove contaminants. RNA was eluted with RNase-free water. The abundance and quality of the resulting RNA was assessed using a Nanodrop ND-1000 spectrophotometer (Nanodrop Technologies, Wilmington, DE, USA). RNA samples were diluted so that 200 ng total RNA could be used for a 25-μl reverse-transcription reaction. cDNA was synthesized using SuperScript II Reverse Transcriptase (Invitrogen).

Quantitative real-time polymerase chain reaction (qRT-PCR). For the quantitative analysis of mRNA expression, the Tecan Sunrise 7500 real-time PCR system (Applied Biosystems, Foster City, CA, USA) was used, with the DNA binding dye SYBR Green (Qiagen) or Taqman (Life Technologies) primers for the detection of PCR products. Each reaction was performed in triplicate using 2 μl of cDNA in a final volume of 20 μl. The following thermal cycle was used for all samples: 10 min-95 °C; 40 cycles of 30 s-95 °C, 40 s-primer specific annealing temperatures, 40 s-72 °C. The melting points, optimal conditions, and specificities of the reactions were first determined using a standard procedure. The expression level of each target gene was analyzed based on the $\Delta\Delta$Ct method and the results expressed as relative expression normalized to 18S or β-actin. Primers for Δ133p53, p53β, and 18S were purchased from Invitrogen and their sequences are as follows: Δ133p53: forward 5′-TGACTTTCAACTCTGTCTCCTTCCT-3′; reverse 5′-GGCCAGACCATCGCTATCTG-3′. p53β: forward 5′-GCGAGCACTGCCCAACA-3′; reverse 5′-GAAAGCTGGTCTGGTCCTGA-3′. 18S: forward 5′-GTAACCCGTTGAA CCCCATT-3′; reverse 5′-CCATCCAATCGGTAGTAGCG-3.′ Taqman primer assays for IL-6, p21, NOS2, IL-1-β, and β-actin were purchased from Life Technologies (sequences available from Life Technologies).

Statistical analysis. Data are presented as mean $\pm$ standard error of the mean (S.E.M.) of an $n=3$ independent experiments unless otherwise stated. Statistical comparisons were made using unpaired two-tailed Student's *t*-test. Differences were considered significant at a value of $^{*}P \leq 0.05$, $^{**}P \leq 0.01$, $^{***}P \leq 0.001$. ImageJ software was used to quantify gel bands from immunoblots using densitometry.

Conflict of Interest

The authors declare no conflict of interest.

Acknowledgements. We thank R Douglas Fields and Bríd Ryan for comments to the manuscript and Kenneth Fischbeck for providing reagents and materials. Confocal microscopy was supported by the National Cancer Institute. Human brain tissues were obtained from the Georgetown University Brain Bank and the Human Brain Collection Core, NIMH. This work was primarily funded by the National Cancer Institute, NIH. CT was supported by the National Institutes of Health-Oxford Scholars Program. BV is supported with projects P206/12/G151 and MEYS—NPS I—LO1413. XL is supported by the Ludwig Institute for Cancer Research Ltd. BTH is partially supported by Georgetown University Brain Bank, NIMH Brain Core, and Target ALS grant.

Author contributions

CT, IH, BTH, and CCH conceived and designed the project. CT, IH, and EF performed the experiments. CT, IH, BTH, and CCH analyzed data. EOM, BV, DPL, and XL provided reagents and guidance on the project. All authors wrote the manuscript.

1. Wimo A, Prince M. *World Alzheimer Report 2010: The Global Economic Impact of Dementia*. Alzheimer's Disease International: London, UK, 2010.
2. Larkindale J, Yang W, Hogan PF, Simon CJ, Zhang Y, Jain A *et al.* Cost of illness for neuromuscular diseases in the United States. *Muscle Nerve* 2014; **49**: 431–438.
3. Barres BA. The mystery and magic of glia: a perspective on their roles in health and disease. *Neuron* 2008; **60**: 430–440.
4. Verkhratsky A, Sofroniew MV, Messing A, deLanerolle NC, Rempe D, Rodríguez JJ *et al.* Neurological diseases as primary gliopathies: a reassessment of neurocentrism. *ASN Neuro* 2012; **4**: 131–149.
5. Furman JL, Sama DM, Gant JC, Beckett TL, Murphy MP, Bachstetter AD *et al.* Targeting astrocytes ameliorates neurologic changes in a mouse model of Alzheimer's disease. *J Neurosci* 2012; **32**: 16129–16140.
6. Das MM, Svendsen CN. Astrocytes show reduced support of motor neurons with aging that is accelerated in a rodent model of ALS. *Neurobiol Aging* 2014; **36**: 1130–1139.
7. Haidet-Phillips AM, Hester ME, Miranda CJ, Meyer K, Braun L, Frakes A *et al.* Astrocytes from familial and sporadic ALS patients are toxic to motor neurons. *Nat Biotechnol* 2011; **29**: 824–828.
8. Jia JP, Meng R, Sun YX, Sun WJ, Ji XM, Jia LF. Cerebrospinal fluid tau, Abeta1-42 and inflammatory cytokines in patients with Alzheimer's disease and vascular dementia. *Neurosci Lett* 2005; **383**: 12–16.
9. Campbell IL, Abraham CR, Masliah E, Kemper P, Inglis JD, Oldstone MB *et al.* Neurologic disease induced in transgenic mice by cerebral overexpression of interleukin 6. *Proc Natl Acad Sci USA* 1993; **90**: 10061–10065.
10. Farina C, Aloisi F, Meinl E. Astrocytes are active players in cerebral innate immunity. *Trends Immunol* 2007; **28**: 138–145.
11. Nagatsu T, Mogi M, Ichinose H, Togari A. Changes in cytokines and neurotrophins in Parkinson's disease. *J Neural Transm Suppl* 2000: 277–290.
12. Tuszynski MH. Nerve growth factor gene therapy in Alzheimer disease. *Alzheimer Dis Assoc Disord* 2007; **21**: 179–189.
13. Erickson KI, Prakash RS, Voss MW, Chaddock L, Heo S, McLaren M *et al.* Brain-derived neurotrophic factor is associated with age-related decline in hippocampal volume. *J Neurosci* 2010; **30**: 5368–5375.
14. Brenner M, Johnson AB, Boespflug-Tanguy O, Rodriguez D, Goldman JE, Messing A. Mutations in GFAP, encoding glial fibrillary acidic protein, are associated with Alexander disease. *Nat Genet* 2001; **27**: 117–120.
15. Miller RG, Mitchell JD, Lyon M, Moore DH. Riluzole for amyotrophic lateral sclerosis (ALS)/ motor neuron disease (MND). *Cochrane Database Syst Rev* 2007; CD001447.
16. Rayess H, Wang MB, Srivatsan ES. Cellular senescence and tumor suppressor gene p16. *Int J cancer* 2012; **130**: 1715–1725.
17. Roninson IB. Oncogenic functions of tumour suppressor p21Waf1/Cip1/Sdi1: association with cell senescence and tumour-promoting activities of stromal fibroblasts. *Cancer Lett* 2002; **179**: 1–14.
18. Debacq-Chainiaux F, Erusalimsky JD, Campisi J, Toussaint O. Protocols to detect senescence-associated beta-galactosidase (SA-betagal) activity, a biomarker of senescent cells in culture and in vivo. *Nat Protoc* 2009; **4**: 1798–1806.
19. Campisi J. Aging, cellular senescence, and cancer. *Annu Rev Physiol* 2013; **75**: 685–705.
20. Sohn JJ, Schetter AJ, Yfantis HG, Ridnour LA, Horikawa I, Khan MA *et al.* Macrophages, nitric oxide and microRNAs are associated with DNA damage response pathway and senescence in inflammatory bowel disease. *PLoS ONE* 2012; **7**: e44156.
21. Wang C, Jurk D, Maddick M, Nelson G, Martin-Ruiz C, von Zglinicki T. DNA damage response and cellular senescence in tissues of aging mice. *Aging Cell* 2009; **8**: 311–323.
22. Coppé J-P, Desprez P-Y, Krtolica A, Campisi J. The senescence-associated secretory phenotype: the dark side of tumor suppression. *Annu Rev Pathol* 2010; **5**: 99–118.
23. Demaria M, Ohtani N, Youssef SA, Rodier F, Toussaint W, Mitchell JR *et al.* An essential role for senescent cells in optimal wound healing through secretion of PDGF-AA. *Dev Cell* 2014; **31**: 722–733.
24. Serrano M. Senescence helps regeneration. *Dev Cell* 2014; **31**: 671–672.
25. Banito A, Lowe SW. A new development in senescence. *Cell* 2013; **155**: 977–978.
26. Storer M, Mas A, Robert-Moreno A, Pecoraro M, Ortells MC, Di Giacomo V *et al.* Senescence is a developmental mechanism that contributes to embryonic growth and patterning. *Cell* 2013; **155**: 1119–1130.
27. Muñoz-Espín D, Cañamero M, Maraver A, Gómez-López G, Contreras J, Murillo-Cuesta S *et al.* Programmed cell senescence during mammalian embryonic development. *Cell* 2013; **155**: 1104–1118.
28. Zilfou JT, Lowe SW. Tumor suppressive functions of p53. *Cold Spring Harb Perspect Biol* 2009; **1**: a001883.
29. Bourdon J-C, Fernandes K, Murray-Zmijewski F, Liu G, Diot A, Xirodimas DP *et al.* p53 isoforms can regulate p53 transcriptional activity. *Genes Dev* 2005; **19**: 2122–2137.
30. Fujita K, Mondal AM, Horikawa I, Nguyen GH, Kumamoto K, Sohn JJ *et al.* p53 isoforms Delta133p53 and p53beta are endogenous regulators of replicative cellular senescence. *Nat Cell Biol* 2009; **11**: 1135–1142.
31. Mondal AM, Horikawa I, Pine SR, Fujita K, Morgan KM, Vera E *et al.* p53 isoforms regulate aging- and tumor-associated replicative senescence in T lymphocytes. *J Clin Invest* 2013; **123**: 5247–5257.
32. Mendrysa SM, Ghassemifar S, Malek R. p53 in the CNS: perspectives on development, stem cells, and cancer. *Genes Cancer* 2011; **2**: 431–442.

33. Kurtkaya-Yapicier O, Scheithauer BW, Hebrink D, James CD. p53 in nonneoplastic central nervous system lesions: an immunohistochemical and genetic sequencing study. *Neurosurgery* 2002; **51**: 1246–1254; discussion 1254–5.
34. Bitto A, Sell C, Crowe E, Lorenzini A, Malaguti M, Hrelia S *et al.* Stress-induced senescence in human and rodent astrocytes. *Exp Cell Res* 2010; **316**: 2961–2968.
35. Surget S, Khoury MP, Bourdon J-C. Uncovering the role of p53 splice variants in human malignancy: a clinical perspective. *Onco Targets Ther* 2013; **7**: 57–68.
36. Horikawa I, Fujita K, Jenkins LM, Hiyoshi Y, Mondal AM, Vojtesek B *et al.* Autophagic degradation of the inhibitory p53 isoform Δ133p53α as a regulatory mechanism for p53-mediated senescence. *Nat Commun* 2014; **5**: 4706.
37. Mizushima N, Yoshimori T, Levine B. Methods in mammalian autophagy research. *Cell* 2010; **140**: 313–326.
38. Tanida I, Ueno T, Kominami E. LC3 and sutophagy. *Methods Mol Biol* 2008; **445**: 77–88.
39. Ferenczy MW, Johnson KR, Steinberg SM, Marshall LJ, Monaco MC, Beschloss AM *et al.* Clonal immortalized human glial cell lines support varying levels of JC virus infection due to differences in cellular gene expression. *J Neuroimmune Pharmacol* 2013; **8**: 1303–1319.
40. Major EO, Miller AE, Mourrain P, Traub RG, de Widt E, Sever J. Establishment of a line of human fetal glial cells that supports JC virus multiplication. *Proc Natl Acad Sci USA* 1985; **82**: 1257–1261.
41. Johansen T, Lamark T. Selective autophagy mediated by autophagic adapter proteins. *Autophagy* 2011; **7**: 279–296.
42. Wu WK, Wu YC, Yu L, Li ZJ, Sung JJY, Cho CH. Induction of autophagy by proteasome inhibitor is associated with proliferative arrest in colon cancer cells. *Biochem Biophys Res Commun* 2008; **374**: 258–263.
43. Pandey UB, Nie Z, Batlevi Y, McCray BA, Ritson GP, Nedelsky NB *et al.* HDAC6 rescues neurodegeneration and provides an essential link between autophagy and the UPS. *Nature* 2007; **447**: 859–863.
44. Tang Y, Horikawa I, Ajiro M, Robles AI, Fujita K, Mondal AM *et al.* Downregulation of splicing factor SRSF3 induces p53β, an alternatively spliced isoform of p53 that promotes cellular senescence. *Oncogene* 2013; **32**: 2792–2798.
45. Bernard H, Garmy-Susini B, Ainaoui N, Van Den Berghe L, Peurichard A, Javerzat S *et al.* The p53 isoform, Δ133p53α, stimulates angiogenesis and tumour progression. *Oncogene* 2013; **32**: 2150–2160.
46. Marcel V, Fernandes K, Terrier O, Lane DP, Bourdon J-C. Modulation of p53β and p53γ expression by regulating the alternative splicing of TP53 gene modifies cellular response. *Cell Death Differ* 2014; **21**: 1377–1387.
47. Marcel V, Dichtel-Danjoy M-L, Sagne C, Hafsi H, Ma D, Ortiz-Cuaran S *et al.* Biological functions of p53 isoforms through evolution: lessons from animal and cellular models. *Cell Death Differ* 2011; **18**: 1815–1824.
48. Haidet-phillips AM, Hester ME, Miranda CJ, Meyer K, Braun L, Frakes A *et al.* Astrocytes from familial and sporadic ALS patients are toxic to motor neurons. *Nat Biotechnol* 2012; **29**: 824–828.
49. Grunseich C, Zukosky K, Kats IR, Ghosh L, Harmison GG, Bott LC *et al.* Stem cell-derived motor neurons from spinal and bulbar muscular atrophy patients. *Neurobiol Dis* 2014; **70**: 12–20.
50. Zhao M, Su J, Head E, Cotman CW. Accumulation of caspase cleaved amyloid precursor protein represents an early neurodegenerative event in aging and in Alzheimer's disease. *Neurobiol Dis* 2003; **14**: 391–403.
51. Kuilman T, Michaloglou C, Mooi WJ, Peeper DS. The essence of senescence. *Genes Dev* 2010; **24**: 2463–2479.
52. Pertusa M, García-Matas S, Rodríguez-Farré E, Sanfeliu C, Cristòfol R. Astrocytes aged in vitro show a decreased neuroprotective capacity. *J Neurochem* 2007; **101**: 794–805.
53. Jiang T, Cadenas E. Astrocytic metabolic and inflammatory changes as a function of age. *Aging Cell* 2014; **13**: 1059–1067.
54. Hefti F. Nerve growth factor promotes survival of septal cholinergic neurons after fimbrial transections. *J Neurosci* 1986; **6**: 2155–2162.
55. Wine RN, McPherson CA, Harry GJ. IGF-1 and pAKT signaling promote hippocampal CA1 neuronal survival following injury to dentate granule cells. *Neurotox Res* 2009; **16**: 280–292.
56. Genis L, Dávila D, Fernandez S, Pozo-Rodrigálvarez A, Martínez-Murillo R, Torres-Aleman I. Astrocytes require insulin-like growth factor I to protect neurons against oxidative injury. *F1000Res* 2014; **3**: 28.
57. Lowe JM, Menendez D, Bushel PR, Shatz M, Kirk EL, Troester MA *et al.* p53 and NF-κB coregulate proinflammatory gene responses in human macrophages. *Cancer Res* 2014; **74**: 2182–2192.
58. Levine AJ, Feng Z, Mak TW, You H, Jin S. Coordination and communication between the p53 and IGF-1-AKT-TOR signal transduction pathways. *Genes Dev* 2006; **20**: 267–275.
59. Gong L, Gong H, Pan X, Chang C, Ou Z, Ye S *et al.* p53 isoform Δ113p53/Δ133p53 promotes DNA double-strand break repair to protect cell from death and senescence in response to DNA damage. *Cell Res* 2015; **25**: 351–369.
60. Ilieva H, Polymenidou M, Cleveland DW. Non-cell autonomous toxicity in neurodegenerative disorders: ALS and beyond. *J Cell Biol* 2009; **187**: 761–772.
61. Marchetto MC, Muotri AR, Mu Y, Smith AM, Cezar GG, Gage FH. Non-cell-autonomous effect of human SOD1 G37R astrocytes on motor neurons derived from human embryonic stem cells. *Cell Stem Cell* 2008; **3**: 649–657.
62. Heuer E, Rosen RF, Cintron A, Walker LC. Nonhuman primate models of Alzheimer-like cerebral proteopathy. *Curr Pharm Des* 2012; **18**: 1159–1169.
63. Muratore CR, Srikanth P, Callahan DG, Young-Pearse TL. Comparison and optimization of hiPSC forebrain cortical differentiation protocols. *PLoS One* 2014; **9**: e105807.
64. Brennand KJ, Simone A, Jou J, Gelboin-Burkhart C, Tran N, Sangar S *et al.* Modelling schizophrenia using human induced pluripotent stem cells. *Nature* 2011; **473**: 221–225.

Supplementary Information accompanies this paper on Cell Death and Differentiation website (http://www.nature.com/cdd)